Journal of Engineering Science and Technology
Vol. 16, No. 4 (2021) 3481 – 3504

REDUCTION OF PAPR PATTERN WITH LOW COMPLEXITY USING HYBRID-PTS SCHEME FOR THE 4G AND 5G MULTICARRIER SYSTEMS

FAWZI M. MUSTAFA*, HUSSAIN M. BIERK, MOHAMMED N. HUSSAIN

Electrical Engineering Department, College of Engineering, Al-Iraqia University, Baghdad, Iraq
*Corresponding Author: fawz60@yahoo.com

Abstract

The cyclic Prefix-Orthogonal frequency division multiplexing (CP-OFDM) system is considered the widespread modulation technology in the innovative fast-moving global communication systems. Many advantages have been recognized the CP-OFDM system compared with the other multicarrier systems such as the high immunity against multipath fading, and the efficiency of bandwidth utilization. However, the frequency leakage, the high peak-to-average power ratio (PAPR) and the signalling synchronization are considered the fundamental snags in the CP-OFDM frameworks. Meanwhile, the PAPR with high value is still the main problem in the 4G and 5G applications. Partials transmit sequence (PTS) is considered part of the techniques to be used to reduce the PAPR that can be utilized to refine the power fluctuation in Filtered-OFDM F-OFDM and CP-OFDM. In the PTS technique, the pseudo-random partitioning scheme (PR-PTS) is the most well-known with the best PAPR reduction scheme. In this work, a hybrid algorithm (H-PTS) has been proposed to decrease the PAPR with high values and with low computational complexity (CC).The H-PTS algorithm combines the PR-PTS scheme and the terminals exchange PTS (TE-PTS) scheme in parallel to produce a hybrid scheme that can significantly reduce the number of mathematical operations and realise a performance reduction in the PAPR higher than the PR-PTS scheme. The simulated results depict that the proposed algorithm has the PAPR behaviour and computational complexity lower than the PR-PTS scheme.

Keywords: CP-OFDM, Computational complexity, F-OFDM, PTS, PR-PTS.

1. Introduction

The cyclic prefix orthogonal frequency division multiplex (CP-OFDM) system and its modifications have become the widespread modulation technology for high-speed transmission rates in the communication frameworks. There are several features that distinguish the CP-OFDM system over the other multicarrier systems, for example, high invulnerability over multipath fading [1], simple execution depending on the Inverse Fast Fourier Transform (IFFT) algorithm [2], and the effectiveness of bandwidth usage [3]. Therefore, the CP-OFDM system has been adopted by many standards of wireless communication like IEEE.802.11 [4], IEEE.802.16 [5], IEEE.802.15 [6], and IEEE.802.20 [7]. Besides, the fourth generation (4G) of cellular wireless standards such as Long-Term Evaluation (LTE) and Worldwide Interoperability for Microwave Access (WiMax) [8] utilizes the CP-OFDM system as the main modulation technique in its operations.

In previous literature, many publications have been published in the context of controlling the PAPR and CC in PTS. Kang et al. [9] suggested the concatenation of the PR-PTS and IL-PTS. Kang's method reduced computation level extensively, but the PAPR scaling down was less than the PR-PTS method. In addition, Wang et al. 10] analysed Kang's method and derived the *CC* equations depending on the concatenate factor. Hong et al. [11] proposed a method that could lessen the *CC* amount by applying PR-PTS to the half of the SBs and IL-PTS to the rest of SBs. The CC level of Hong's method is reduced better than PR-PTS; however, the PAPR reduction capacity is degraded compared to PR-PTS. Moreover, Chen and Chung [12] presented a modified PTS algorithm by reshaping a quadrature amplitude modulation (QAM) constellation block into several quadrature phase-shift keying (QPSK) constellation blocks and then employing the SBs partition scheme. The Chen's method of PAPR reduction is slightly superior to the PR-PTS scheme, while the CC level is like that of PR-PTS with a slight degradation in the BER performance. In addition, Fulai et al. [13] reduced the PAPR value by combining the discrete Fourier transform spread (DFT-S) and PTS.

The PAPR lessening capacity of Fulai's et al. approach outdoes the traditional PTS scheme because the DFT-spread can make divergence in the autocorrelation between subchannels, but this improvement comes at the cost of more mathematical calculations. Similarly, Jayashri et al. [14] initiated the combination of discrete-cosine-transform spread (DCT-S) and PTS technique such that the PAPR can be mitigated in the traditional CP-OFDM structure. The PAPR level of Jayashri's et al. method is superior to PR-PTS due to the influence of DCT-S, whereas the CC level is higher than the traditional PR-PTS scheme. Lim et al. [15] putted another strategy for diminishing the *CC* level of the PTS method. Lim's method depended on two stages of the IFFT transformation for reducing the *CC* level. The PAPR diminishing performance of Lim's strategy is closely corresponding to that of the PR-PTS technique with low *CC*. Wang and Cao [16] proposed an effective method for reducing the *CC* level by employing the linear property of IFFT. The number of mathematical operations of L. Wang approach is less than the PR-PTS method at the cost of degradation in the PAPR lessening capacity. Recently, Y. Jawhar et al. in [17-19] proposed new subblocks dividing schemes in PTS for reducing the PAPR value and the *CC* level.

Based on the literature review, it can be noted that the PR-PTS method is the preeminent distinguished SBs partitioning scheme in terms of PAPR performance

reduction, and there is a trade-off between the numbers of *CC* in the PTS method and the PAPR improvement capacity.

In this paper, a new combination approach is introduced for improving the PAPR reduction performance better than the PR-PTS method with a low *CC* level by combining the PR-PTS method and proposed method in [20]. The rest parts of the paper are structured as follows: Section 2 analyses the OFDM and F-OFDM systems. Section 3 explains the PTS strategy. Section 4 explains the conventional SBs partitioning schemes. The proposed method is introduced in Section 5. The *CC* analysis is explained in Section 6. Section 7 discusses the results. Finally, the study conclusions were drawn out in Section 8.

2. CP-OFDM and F-OFDM

In the CP-OFDM, the input symbols are baseband-modulated firstly according to one of the modulation standards, for instance, QAM or PSK. The IFFT function is used to convert the modulated symbols X_k,{k= 0, 1, 2, …, N-1} from the frequency domain (FD) into the time domain (TD) to produce the discrete baseband OFDM signal x(n), which can be presented as [21],

$$x(n) = \frac{1}{\sqrt{N}} \sum_{k=0}^{N-1} X_k e^{j2\pi k \frac{n}{N}} \quad , \quad \mathrm{n} = 0, 1, 2, \ldots, N-1 \tag{1}$$

where N symbolizes the subcarriers number. Generating the discrete baseband OFDM signal occur by superposition the K-samples of the input data symbol with N-subcarriers in orthogonally. In the OFDM, performing the cycle prefix insertion by adding the last part of the OFDM signal in front of the OFDM symbol to prevent the inter-symbol-interference (ISI) from occurring to the signal [22]. On the other hand, the construction of the OFDM signal is performed by combining the N-modulated subcarriers together. Therefore, there may be an increase in the power of some samples overriding the average power of the signal when the samples phases are similar. Hence, the PAPR value can be represented as the rate of the maximum instantaneous power divided by the signal mean power and can be presented as [23],

$$\mathrm{PAPR} = \frac{\max|x(n)|^2}{E\{|x(n)|^2\}} \tag{2}$$

where $E\{.\}$ represents the mean value. Moreover, the complementary cumulative distribution function (CCDF) is generally utilized to evaluate the PAPR values probability that exceeds a specific threshold value [24].

$$Pr(\mathrm{PAPR} > PAPR_0) = 1 - (1 - \exp(-PAPR_0))^{NL} \tag{3}$$

where $PAPR_0$ represents the threshold value, and L stands for the oversampling factor which makes the discrete time signal the similar to the characteristic of the continuous time signal, this is finished by embedding (L-1) N zeros in the FD samples [3].

In F-OFDM system, the CP-OFDM signal is filtered by the transmitter filter before transmitting, and the same type of the filter is utilized at the receiver side. Figure 1 demonstrates the F-OFDM system diagram, where the transmitted signal after the CP-OFDM processing is passed through the transmitter filter $f(n)$ to generate the transmitter F-OFDM signal. However, the receiver of F-OFDM signal is passed initially to the filter $f^*(-n)$ receiver, which is corresponding to the

transmitter spectrum shaping filter [25]. The receiver filter protects the received signal from the adjacent signals. Hereafter, the receiver filter rejects any contributions of the other signals and ensures the CP-OFDM signal is transferred successfully to the next phase avoiding the interference from the adjacent signals [26]. Adding the filter to the system increases the complexity and it increases the PAPR value of the F-OFDM higher than CP-OFDM because the added filter makes the power distribution among the samples wider than the CP-OFDM system and this leads to reducing the signal mean power. Therefore, the F-OFDM system suffers from increasing in the PAPR value and the *CC* level.

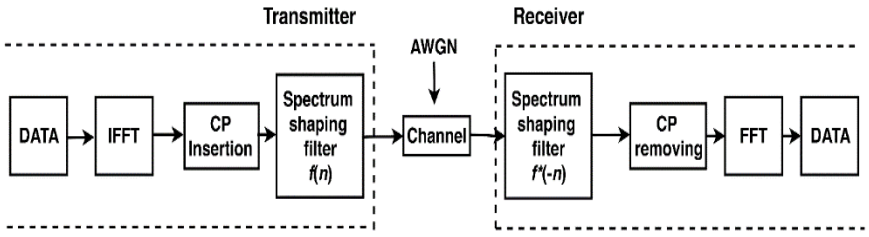

Fig. 1. Block diagram of F-OFDM [25].

Moreover, the filter design plays an essential role to achieve the needed flexibility between the frequency and time localization, which is an important feature in the 5G applications [27]. Besides, the significant features of the Sinc impulse response filter of being able to suppress OOBE without distorting the passband of the signal, makes it suitable spectrum shaping filter to be implemented in F-OFDM. Moreover, to ensure of the smooth transfer for the filter impulse response both ends in the TD and to offer a good time localization, the windows mask is implemented [28]. The rooted raised cosine (RRC) window appeared more appropriate for F-OFDM due to its higher flexibility compared to another window for instance, Wu et al. [29]. Therefore, of the RRC window filter time response is formulated as [30]

$$w_{RRC}(n) = \left[0.5\left(1 + \cos\left(\frac{2\pi n}{FL-1}\right)\right)\right]^{\alpha} \quad (4)$$

where *FL* represents the length of the filter, and α symbolizes the roll-off factor that controls the window shape. The filter length of F-OFDM is let to exceed the cyclic prefix length to achieve better balance in terms of localization between the time and frequency and to accomplish more flexible filter design [31].

3. Conventional PTS (C-PTC)

PTS is considered an effective scenario to reduce the PAPR value without signal distortion because it is probabilistic method [17]. Figure 2 illustrates the C-PTS concept, where the data sequence is segmented to V- subblocks,

$$X = \sum_{v=1}^{V} X_v \quad (5)$$

where the number of SBs is represented by *V*. After that, the portioned SBs are transferred to the N-IFFT blocks to modulate the baseband data with the subcarriers orthogonally. After that, the SBs in the TD are timed by a set of phase factor vectors

(b_v) component-wise, to result with a group of candidate sequences, thus the OFDM signal takes the form,

$$x = IFFT\{\sum_{v=1}^{V} b_v X_v\} \quad (6)$$

Finally, the candidate combination having the lowest value of the will be adopted for transmission. That is, the output OFDM signal that utilizes the PTS technique can be expressed as [18]

$$OFDM\ signal = \sum_{v=1}^{V} b_v^{\text{opt}} x_v \quad (7)$$

where the best phase rotation sequence is represented by b_v^{opt}, which is usually limited to $b_v \in \{\pm 1\}$ or $\{\pm 1, \pm j\}$ to decrease the complex multiplications [31]. The phase rotation factors can be obtained as

$$b_v = \left\{e^{j2\pi v/W} | v = 0,1,\ldots\ldots, W-1\right\} \quad (8)$$

where W symbolizes the permissible phase rotation factors number. In addition, the optimum phase weighting factors can be found by using the following optimization expression [32],

$$\{b_1, b_2, \ldots, b_V\} = \underset{1 \le w \le W}{\text{argmin}} \left(\underset{0 \le n \le NL-1}{\text{max}} | \sum_{v=1}^{V} b_v x_v | \right) \quad (9)$$

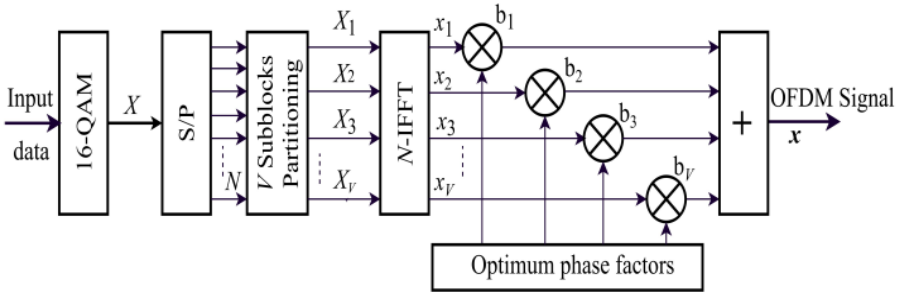

Fig. 2. Block diagram of the C-PTS in the transmitter [17].

In C-PTS, the system should perform a comprehensive search to determine the optimum phase rotation factor, so this operation imposes a high *CC* level, and it requires high processing time. Moreover, the transmitter side should send ($\log_2 WV$-1) bits per symbol as side information to regain the transmitted signal in the receiver sideways [18].

4. The conventional partitioning schemes

As mentioned, the three well-known partitioning schemes include adjacent, interleaving and pseudo-random scheme. The segmentation schemes work to reduce the correlation between the input samples of the data sequence; therefore, in each scheme, there is a PAPR reduction gain and *CC* level different than each other. In PR-PTS, the active subchannels are allocated inside the SBs randomly, whereas Ad-PTS allocates the successive subcarriers into the SBs sequentially, while IL-PTS assigns each active subcarrier within a certain interval (V) inside the SBs, as demonstrated in Fig. 3.

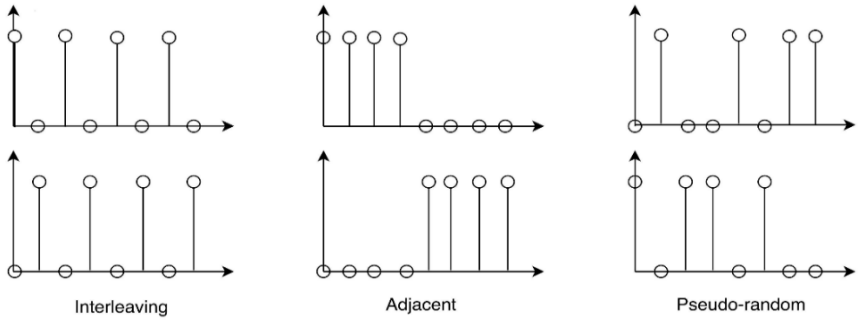

Fig. 3. The conventional segmentation schemes [19].

In terms of the PAPR reduction evaluation, the PR-PTS algorithm is regarded the best scheme among the conventional algorithms, and Ad-PTS is considered the second scheme in terms of efficiency, while IL-PTS is the worse among the partitioning schemes [11]. This can be attributed to the autocorrelation nature between subcarriers within subblocks [33]. On the other hand, Ad-PTS and PR-PTS have a larger number of mathematical operations compared with IL-PTS, because they implement the entire IFFT stages when converting their samples to the TD. However, IL-PTS requires a fewer IFFT phases to perform the transformation of samples to the TD because of the interleaving nature. Therefore, complex multiplication and addition operations of PR-PTS or Ad-PTS can be formulated as [9],

$$C_{\text{add}}^{\text{PR/Ad}} = V[N\, log_2\, N] \tag{10}$$

and,

$$C_{\text{mult}}^{\text{PR/Ad}} = V[\frac{N}{2} log_2\, N] \tag{11}$$

Also, the complex multiplication and addition of IL-PTS when performing the Cooley-Tukey IFFT approach can be calculated as [17],

$$C_{\text{add}}^{\text{IL}} = V[\frac{N}{V} log_2 \frac{N}{V}] \tag{12}$$

and,

$$C_{\text{mult}}^{\text{IL}} = V[\frac{N}{2V} log_2 \frac{N}{V} + N] \tag{13}$$

5. The Proposed Technique

In this proposed technique, the PR-PTS scheme is combined with a new segmenting plan defined as terminals exchange PTS (TE-PTS) scheme that published in [20] to refine both PAPR reduction and *CC* level. The proposed method combines PR-PTS and TE-PTS in parallel, so it is called the hybrid PTS (H-PTS) scheme.

5.1. The TE-PTS scheme

The TE-PTS scheme is suggested to smooth the PAPR lessening work to outperform the IL-PTS scheme without degradation in the *CC* level [20]. The TE-

PTS scheme depends on the IL-PTS technique primarily, where $X(k)$ as data sequence is subdivided to V subblocks like IL-PTS,

$$X(k) = \sum_{v=1}^{V} X_v^{\mathrm{IL}} \tag{14}$$

where X_v^{IL} represents the v^{th} SB of the IL-PTS matrix. After that, each new partition is further partitioned to R subsets, denoted by $\{R1, R2, \ldots, RV\}$, such that $R=V$, and each subset contains N/V samples from the SB samples. Afterward, the first and last samples of each subset are exchanged with each other, and the terminals exchange operation proceeds to the last subset of updated IL-PTS matrix. At last, the distribution of the sample inside the SBs are reshaped in a new scheme [20]. Hence, the input data sequence based on the TE-PTS scheme is,

$$X(k) = \sum_{v=1}^{V} X_v^{\mathrm{TE}} \tag{15}$$

where stands for the v^{th} SB of the TE-PTS matrix. Figure 4 depicts an example of TE-PTS. A number of SBs was chosen as four, while there are sixteen subchannels. Depending on the TE-PTS approach, the total number of the subset, R, is determined to 4, denoted by $\{R1, R2, R3, R4\}$, and each subset contains (N/V =16/4=4) samples. It is notable that the TE-PTS scheme reshapes the distribution of the sample inside the SBs differently compared with the IL-PTS scheme. Accordingly, the TE-PTS scheme leads to reducing the correlation amount between subchannels compared with the IL-PTS algorithm [20]. Therefore, the performance reduction of PAPR will be improved.

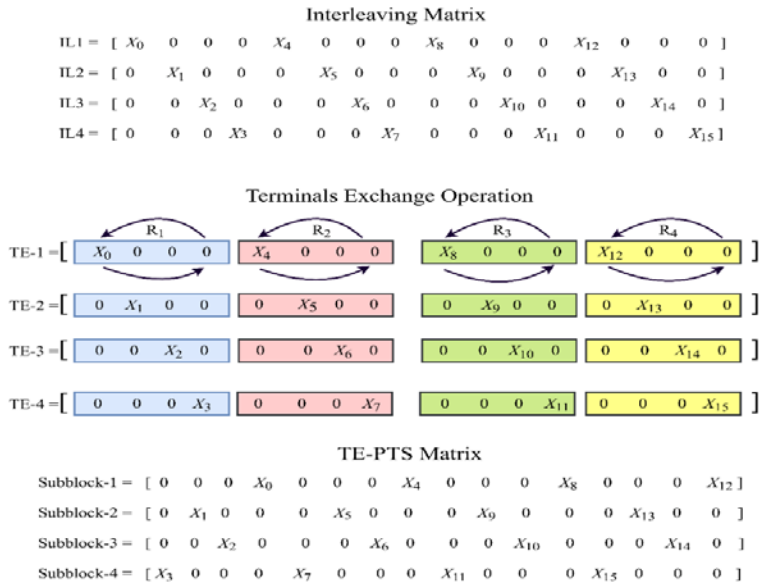

Fig. 4. TE-PTS scheme when N=16 and V=4 [20].

5.2. The PR-PTS scheme

As aforementioned, the finest methodology among the partitioning approaches in terms of PAPR reduction gain is the PR-PTS scheme. This is because the random distribution of its subcarriers within the SBs, which leads to decreasing the

correlation between the subcarriers [33]. In contrast, the PR-PTS scheme implements all the IFFT stages to modulate the SBs; thus, its computational load level is higher with respect to other methods. Figure 5 shows the subcarrier distributions inside SBs in the PR-PTS way.

$$X(k) = [\ X_0\ X_1\ X_2\ X_3\ X_4\ X_5\ X_6\ X_7\ X_8\ X_9\ X_{10}\ X_{11}\ X_{12}\ X_{13}\ X_{14}\ X_{15}\ ]$$

PR-PTS Scheme

$$V1 = [\ 0\ 0\ 0\ X_3\ 0\ 0\ 0\ 0\ X_8\ X_9\ 0\ X_{11}\ 0\ 0\ 0\ 0\ ]$$

$$V2 = [\ X_0\ 0\ 0\ 0\ 0\ X_5\ 0\ X_7\ 0\ 0\ X_{10}\ 0\ 0\ 0\ 0\ 0\ 0\ ]$$

$$V3 = [\ 0\ 0\ X_2\ 0\ 0\ 0\ X_6\ 0\ 0\ 0\ 0\ 0\ 0\ 0\ X_{14}\ X_{15}]$$

$$V4 = [\ 0\ X_1\ 0\ 0\ X_4\ 0\ 0\ 0\ 0\ 0\ 0\ 0\ X_{12}\ X_{13}\ 0\ 0\ ]$$

Fig. 5. The PR-PTS scheme when *V*=4 and *N*=16.

5.3. The H-PTS scheme

As mentioned in the first part of this section, the H-PTS algorithm merges the PR-PTS scheme and the TE-PTS scheme in parallel to produce a hybrid scheme which can reduce significantly the number of mathematical operations and accomplishes a performance reduction in the PAPR superior to the PR-PTS scheme. Therefore, the H-PTS algorithm is suggested in order to make use of the high PAPR diminishing capability of PR-PTS and the low *CC* feature of the TE-PTS scheme.

Figure 6 demonstrates the H-PTS algorithm, where the first step starts at dividing the input data set X to two parts, X^A and X^B,

$$X = \{X^A, X^B\} \tag{16}$$

where X^A represents the first part of the input data symbol and contains the half subcarriers of the input data sequence, while the second part X^B consists of the rest of the subcarriers. Therefore, the first part of the input data sequence X^A is,

$$X^A = [X_0, X_1, \ldots, X_{(N/2)-1}] \tag{17}$$

However, the second part of the input symbol X^B is written as

$$X^B = [X_{(N/2)}, X_{(N/2)+1}, \ldots, X_{N-1}] \tag{18}$$

After that, the first part X^A undergoes the PR-PTS scheme, whereas the X^B part undergoes the TE-PTS scheme, where the data sequence in each part is divided into V subblocks,

$$X^A = \sum_{v=1}^{V} X_v^A \tag{19}$$

and,

$$X^B = \sum_{v=1}^{V} X_v^B \tag{20}$$

Finally, each SB of the partitioned parts (X^A and X^B) is fed to N/2-*IFFT* block, and the phases of each part are optimized before combining again to produce the hybrid OFDM signal (x^H),

$$x_{(n)}^A = IFFT\{\sum_{v=1}^{V} b_v^A X_v^A\} = \sum_{v=1}^{V} b_v^A x_v^A \quad \text{, where } 0 \le n \le (N/2)\text{-}1 \tag{21}$$

and,

$$x_{(n)}^{B}=IFFT\{\sum_{v=1}^{V} b_v^B X_v^B\} = \sum_{v=1}^{V} b_v^B x_v^B \quad , \text{ where } (N/2) \leq n \leq N\text{-}1 \tag{22}$$

then,

$$x_{(n)}^{H} = \{b^A x^A, b^B x^B\}, \text{where } 0 \leq n \leq N\text{-}1 \tag{23}$$

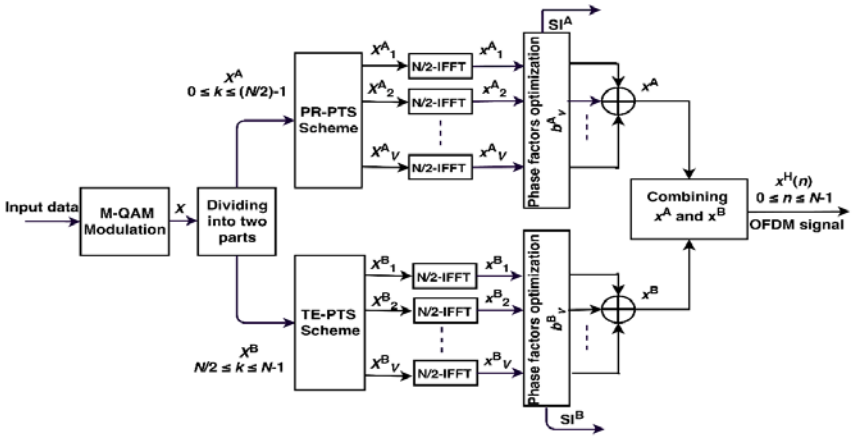

Fig. 6. The H-PTS scheme block diagram transmitter side.

In the H-PTS algorithm, the first part of the algorithm is utilized based on the PR-PTS scheme, which can achieve a superiority PAPR performance reduction at the cost of increasing in the calculations burden, whereas the other part of the algorithm is integrated with the TE-PTS scheme which can accomplish a good reduction in PAPR capacity with lower computational complexity. Moreover, the phases of each part of the signal are optimized separately to produce the optimum candidate signal before combining both parts again in the TD. Accordingly, the H-PTS algorithm can fulfil a PAPR reduction gain superior to PR-PTS, which is considered the most common significant scheme to boost the PAPR performance level in PTS.

6. The Analysis of Computational Complexity

The H-PTS scheme's computational complexity includes the mathematical calculations of the algorithm in the FD and the TD. The former represents the number of summations and multiplications operations in the IFFT units for both the TE-PTS and the PR-PTS schemes, while the latter represents the number of the multiplication's number and addition processes to determining the optimum phase rotation factor for every portion in the H-PTS algorithm.

6.1. The computational complexity in the frequency domain

This *CC* level signifies the number of addition and multiplications that have been performed in the IFFT units when transforming the subblocks from the FD into the TD. Therefore, this complexity includes the IFFT calculations of the TE-PTS and PR-PTS schemes, as follows.

6.1.1. The complexity of the TE-PTS scheme

The *CC* level of TE-PTS can be determined depending on the divide-and-conquer method joint with the Cooley-Tukey IFFT algorithm [20]. In every SB of the TE-PTS matrix, the samples are arranged in columns-wise mapping as drawn in Table 1. Hence, the number of subsets, *M*, defines the total number of subdivides in one subblock of the TE-PTS fashion, while the rows equal the number of *SB*s, *V*, in TE-PTS scheme.

Table 1. The columns-wise mapping for subblock in the TE-PTS scheme [20].

v \ ***m***	**0**	**1**	**2**	**…**	***M* -1**
0	*X*(0)	*X*(*V*)	*X*(2*V*)	…	*X*((*M* -1)*V*)
1	*X*(1)	*X*(*V*+1)	*X*(2*V*+1)	…	*X*((*M* -1)*V*+1)
2	*X*(2)	*X*(*V*+2)	*X*(2*V*+2)	…	*X*((*M* -1)*V*+1)
…	…	…	…	…	…
V-1	*X*(*V*-1)	*X*(2*V*-1)	*X*(3*V*-1)	…	*X*(*MV* -1)

The TD signal after performing the Cooley-Tukey IFFT algorithm on columns and rows in Table 1 can be formulated as [30],

$$x(p,q) = \frac{1}{\sqrt{N}} \sum_{v=0}^{V-1} \left\{ W_N^{vq} \left[\sum_{m=0}^{M-1} X(v,m) W_M^{mq} \right] \right\} W_V^{vp} \tag{24}$$

where *M* the columns total number in Table 1, *V* is rows total number in Table 1, *X*(*v*,*m*) is the input sequence of mth subblock, $1 \leq p \leq V$ and $1 \leq q \leq M$ is an element in p^{th} row and q^{th} column of row-wise mapping of the *x*(*p*,*q*), and represents the twiddle factor. Equation (24) represents the calculation of the IFFT unit for the rectangular array of length *V* and width *M*. Because of the column-wise mapping and the periodic property of the TE-PTS scheme, the active subcarriers of each subblock are placed at only vth row of the column-wise table, as shown in Fig. 7. Therefore, inner *M*-point IFFT is implemented only at v^{th} row, and (24) is simplified as

$$x(p,q) = \frac{1}{\sqrt{N}} \left\{ W_N^{vq} \; W_V^{vp} \left[\sum_{m=0}^{M-1} X(v,m) W_M^{mq} \right] \right\} \tag{25}$$

but $W_V^{vp} = 1$, if $V = 1$; thus,

$$x(p,q) = \frac{1}{\sqrt{N}} \left\{ W_N^{vq} \left[\sum_{m=0}^{M-1} X(v,m) W_M^{mq} \right] \right\} \tag{26}$$

Consequently, each subblock of TE-PTS scheme needs to calculate N-times complex multiplications and only one M-point IFFT and N-times complex multiplications. Therefore, the total complex additions in TE-PTS are,

$$C_{\text{add}}^{\text{TE-PTS}} = V[M \log_2 M] \tag{27}$$

but, $M = N/V$; then,

$$C_{\text{add}}^{\text{TE-PTS}} = V \left[\frac{N}{V} \log_2 \frac{N}{V} \right] \tag{28}$$

Also, if the Cooley-Tukey IFFT algorithm is used, the complex multiplications quantity in TE-PTS fashion equals half of the number of the complex additions. Therefore, the multiplication's load is calculated as

$$C_{\text{mult}}^{\text{TE-PTS}} = V\left[\left(\frac{M}{2} log_2 M\right) + N\right] \tag{29}$$

then,

$$C_{\text{mult}}^{\text{TE-PTS}} = V\left[\left(\frac{N}{2V} log_2 \frac{N}{V}\right) + N\right] \tag{30}$$

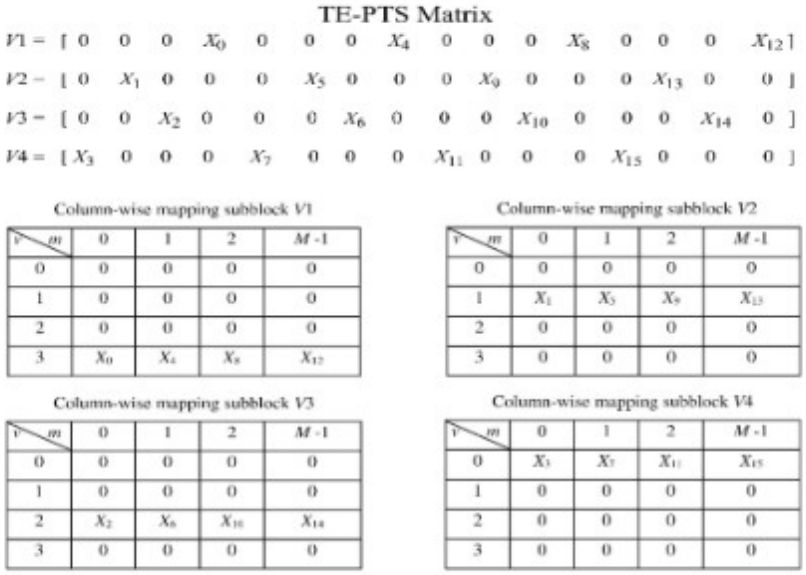

Fig. 7. Column-wise mapping of IL-PTS when *N*=16 and *V*=4.

It is clear that the *CC* level of the TE-PTS scheme is similar to the IL-PTS scheme, this is due to the subcarriers for both schemes are distributed as interleaving manner within the SBs. Hence, the SBs require a part of the IFFT stages for converting the subcarriers to the TD.

6.1.2. The complexity of the PR-PTS scheme

The PR-PTS scheme's CC level is calculated based on the Cooley-Tukey IFFT algorithm, where the active subcarriers are distributed randomly inside the SBs. Hence, the PR-PTS scheme requires to deploy the whole IFFT phases for transforming the SBs into the TD. Hence, the number of addition and multiplication processes in PR-PTS are given in (10) and (11) respectively.

6.2. The computational complexity in the time domain

In the CP-OFDM system, the *CC* level in the TD represents the number of operations to reach the optimum phase rotation factor in the PTS method. Therefore, the number of complex multiplications and additions that are needed to optimize the phases in the TE-PTS or PR-PTS scheme can be given as [34]

$$C_{\text{add/CP-OFDM}}^{\text{TE-PTS/PR-PTS}} = W^{V-1} \times N \times (V-1) \tag{31}$$

and,

$$C_{\text{mult/CP-OFDM}}^{\text{TE-PTS/PR-PTS}} = W^{V-1} \times N \times (V+1) \tag{32}$$

In F-OFDM system, while measuring the *CC* level in TD , and when comparing it with CP-OFDM, it can be seen that it has lower *CC* level in TD than the F-OFDM due to the extra calculations resulted from the added filter in the transmitter. This extra *CC* results from the multiplication of the filter length and the CP-OFDM; Therefore, F-OFDM system results with higher number of complex additions [35]. There is a match between the number of complex additions of F-OFDM and CP-OFDM [36]. Therefore, the multiplication and addition operations amount of the F-OFDM system in the TD are calculated as

$$C_{\text{mult/F-OFDM}}^{\text{TE-PTS/PR-PTS}} = C_{\text{mult}}^{\text{TE-PTS/PR-PTS}} + \text{filter complexity} \tag{33}$$

then,

$$C_{\text{mult/F-OFDM}}^{\text{TE-PTS/PR-PTS}} = W^{V-1} \times N \times (V+1) + [N \times (FL-1)] \tag{34}$$

6.3. The computational complexity of the H-PTS scheme

The H-PTS algorithm *CC* level represents the number of the complex multiplications and additions in the FD and the TD based on the structure of the H-PTS algorithm. Henceforth, the total number of the computational complexity computations of the H-PTS scheme in the transmitter side is to sum the *CC* level of both combined schemes, TE-PTS and PR-PTS, which can be written as

$$C_{\text{CP-OFDM}}^{\text{H-PTS}} = \text{frequency domain complexity} + \text{time domain complexity} \tag{35}$$

then,

$$C_{\text{add/CP-OFDM}}^{\text{H-PTS}} = \frac{V}{2}\left[\left(N \log_2 \frac{N}{2}\right) + \left(\frac{N}{V} \log_2 \frac{N}{2V}\right)\right] + [W^{V-1} \times N \times (V-1)] \tag{36}$$

and,

$$C_{\text{mult/CP-OFDM}}^{\text{H-PTS}} = \frac{V}{2}\left[\left(\frac{N}{2} \log_2 \frac{N}{2}\right) + \left(\frac{N}{2V} \log_2 \frac{N}{2V}\right) + \frac{N}{2}\right] + [W^{V-1} \times N \times (V+1)] \tag{37}$$

6.4. The side information bits of the H-PTS scheme

The overhead bits are the number of bits that are transferred to inform the receiver about the index of the utilized phase rotation factors so as to recover the original data at the receiver [18]. The side information bits in the H-PTS algorithm represent the bits number of side information for the first part (SIA) and the number of side information for the second part (SIB). Therefore, the bits of the side information of the proposed algorithm (SIH-PTS) are formulated as,

$$SI^{\text{H-PTS}} = SI^{A} + SI^{B} \tag{38}$$

then,

$$SI^{\text{H-PTS}} = log_2 W^{V-1} + log_2 W^{V-1} \tag{39}$$

thus,

$$SI^{\text{H-PTS}} = 2\, log_2 W^{V-1} \tag{40}$$

7. Results and Discussion

7.1. PAPR evaluation

In the H-PTS algorithm, the PR-PTS scheme and the TE-PTS scheme are combined in parallel to produce a hybrid scheme that can accomplish a PAPR lessening performance better than that of the PR-PTS algorithm and reduce the computational complexity level significantly. In the H-PTS scheme, the CCDF will be examined when N=64 and 128 points, while the baseband modulation 4-QAM and 16-QAM, respectively. Moreover, the number of cyclic prefix CP=36, L=4, V=4, W=4, the cyclic prefixes number CP=36, and the filter length FL=257. Also, the H-PTS algorithm will apply to the CP-OFDM and F-OFDM for evaluating the BER and PAPR performances according to the AWGN channel.

In the CP-OFDM system, the size of the OFDM symbol and the consultation mapping have been chosen 64 and 4-QAM, which correspond to IEEE802.11a/g/n, IEEE802.11ad, IEEE802.11ah, and the IEEE802.15 group in the wireless communication systems. As can be seen from Fig. 8, when W=4, and V=4, the H-PTS scheme is better than PR-PTS and the other suggested algorithms in literature, where the PAPR value was 6.21 dB for H-PTS, 6.36 dB for Jayashri's et al. method [14], 6.4 dB for Fulai's et al. method [13], 6.49 dB for H. Chen and Chung's method [12], 6.54 dB for PR-PTS, 6.74 dB for Kang's et al. method [9] or Wang's et al. method [10], 7.02 dB for Wang's et al. method [16], 7.23 dB for Hong's et al. method [11], and 10.5 dB for the CP-OFDM original signal.

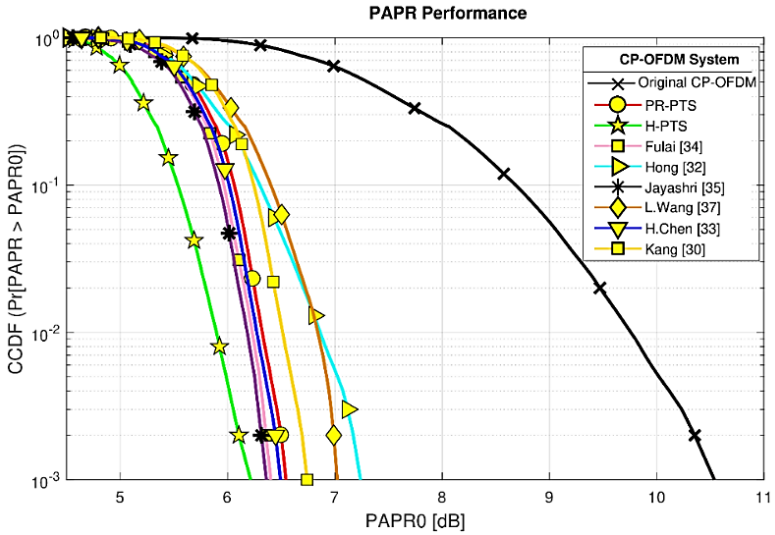

Fig. 8. CCDF for the H-PTS scheme and some of the suggested techniques in literature in the CP-OFDM system, N = 64, 4-QAM.

Furthermore, Fig. 9 presents the BER performance of the H-PTS scheme compared with the OFDM original signal, where both signals BER gain is identical because of the probabilistic nature of H-PTS. In other words, the H-PTS maintains the constellation points of the signal without change.

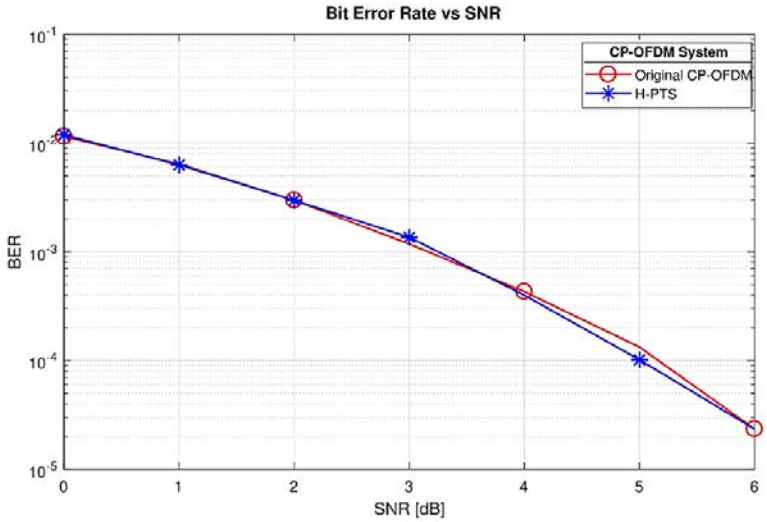

Fig. 9. BER for the H-PTS scheme in CP-OFDM system, *N*=64, 16-QAM.

Likewise, the simulation is executed with the IFFT size equals 128, and the constellation mapping is 16-QAM, as depicted in Fig. 10. The simulated results indicate that the PAPR value was 6.87 dB for H-PTS, 6.98 dB for Fulai's et al. method, 6.99 dB for Jayashri's et al. method, 7.03 dB for Chen and Chung's method, 7.11 dB for PR-PTS, 7.3 dB for Kang's et al. method or Wang's et al. method, 7.37 dB for Lim et al. method [15], 7.5 dB for Hong's et al. method, 7.7 dB for Wang's et al. method, and 10.8 dB for CP-OFDM signal. Again, the H-PTS scheme keeps the BER gain without degradation as compared to the OFDM original signal, as displayed in Fig. 11.

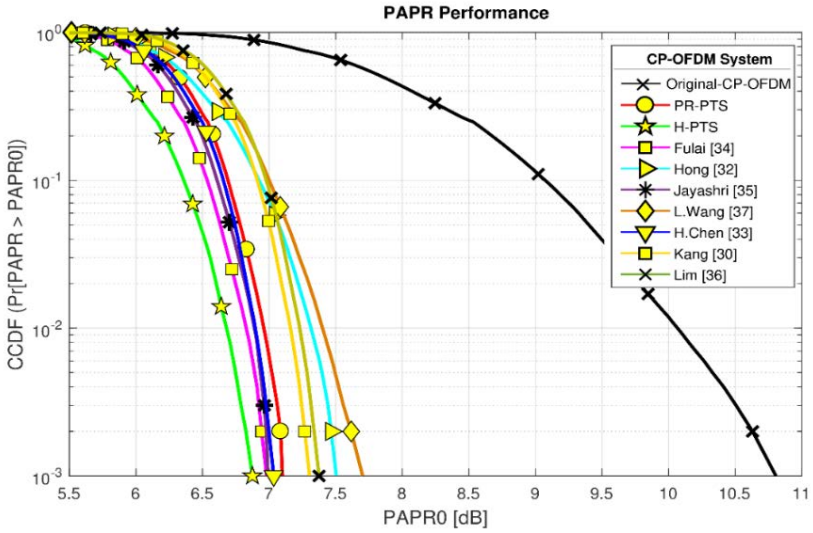

Fig. 10. CCDF for the H-PTS scheme and some the suggested methods in literature in CP-OFDM system, *N*=128, 16-QAM.

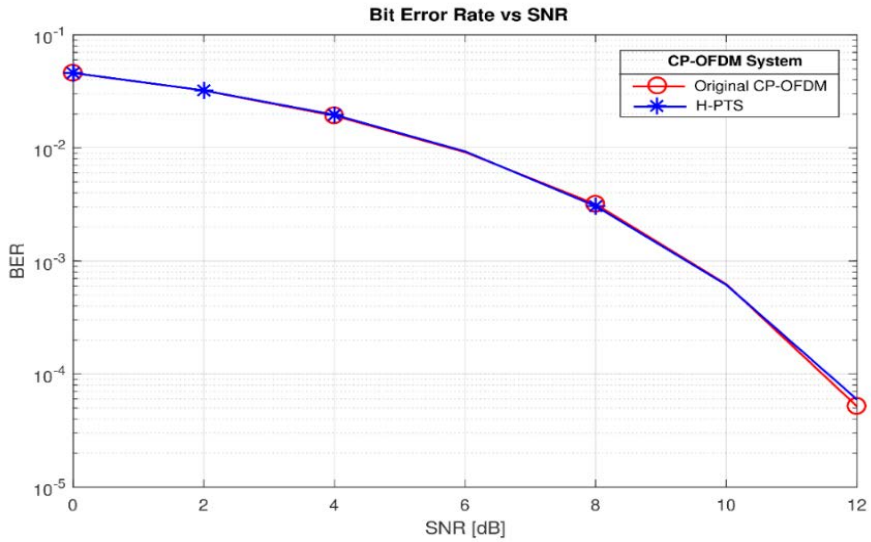

Fig. 11. BER for the H-PTS scheme in CP-OFDM system, N = 128, 16-QAM.

In brief, the proposed algorithm, H-PTS, can enhance the reduction performance of the PAPR better than that of the PR-PTS which is considered the best well-known scheme to decrease the PAPR pattern in the PTS technique. Furthermore, the proposed algorithm exceeds the other previously proposed methods in the literature regarding PAPR reduction capacity. The reason behind that is the H-PTS algorithm divides the input data sequence into two-part, and the data of these parts are processed by different schemes PR-PTS and TE-PTS. Hence, the long correlation level between the samples is broken-down better than other schemes accordingly. Moreover, the converted SBs of each part in the TD are weighted by two sets of the phase rotation factors, in other words, the optimum phase factors of the first part differ to that of the second part. Therefore, the correlation peak here is lower than the correlation peak when one set of the phase factors is used for weighting the whole data sequence. Besides, the BER performance of the proposed technique is maintained without degradation due to the algorithm is built based on the multiple signal representations technique that has been adopted in the PTS technique.

In the F-OFDM system, the two schemes of H-PTS and PR-PTS have been compared with respect to the F-OFDM and CP-OFDM system. The simulation parameters are defined as: N=128, 16-QAM, L=4, V= 4, W=4, FL=257, CP=36, and α=0.6. Figure 12 depicts the diminishing performances of the PAPR of H-PTS, and the PR-PTS scheme according to CP-OFDM and F-OFDM systems. The H-PTS based on CP-OFDM is better than the same scheme based on F-OFDM by 1.72 dB, while the difference in the PAPR value for the PR-PTS schemes by using both systems is 1.72 dB. Moreover, the original signal based on CP-OFDM exceeds that the F-OFDM system by 1.64 dB. This differences in PAPR performances is due to the transmitter filter leads to decreasing the signal's mean power, thus the PAPR performance has been degraded accordingly. In addition, the BER performances of H-PTS and the original signal based on F-OFDM is compared in Fig. 13. It has been found that the BER performance of the H-PTS is almost the same as the original F-OFDM signal. For instance, the probability of error for the H-PTS scheme-based F-

OFDM is 2.56×10-3 at 10 dB of SNR, while the original F-OFDM BER value is 2.08×10-3 at 10 dB of SNR.

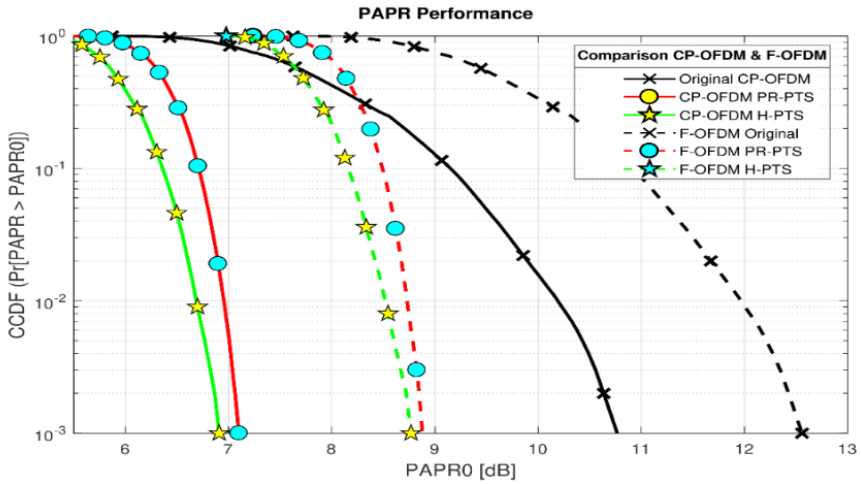

Fig. 12. PAPR comparison based on CP-OFDM and F-OFDM for the original signal, H-PTS, and PR-PTS schemes, *N*=128, *M*=16.

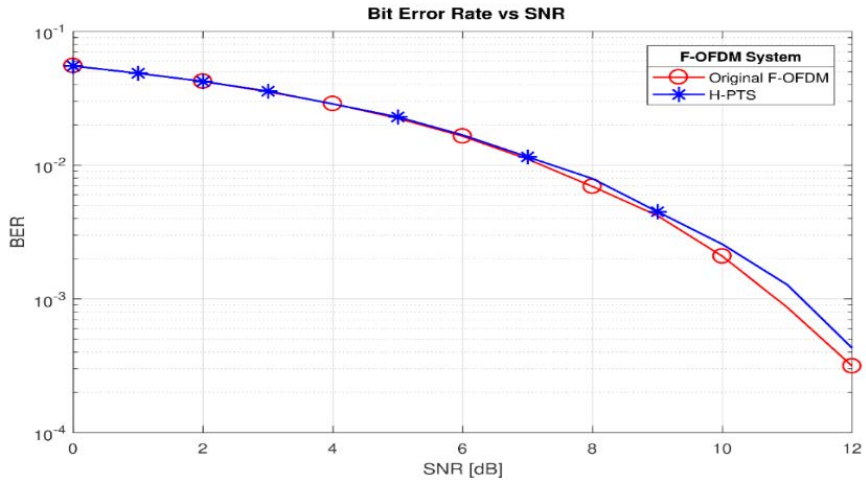

Fig. 13. BER for the H-PTS scheme in F-OFDM, *N*=128, *M*=16.

Besides, the comparison of the BER performance between the CP-OFDM and F-OFDM systems according to the H-PTS scheme has been conducted, as shown in Fig. 14. It is obvious that the H-PTS scheme of the F-OFDM outperforms the BER gain of the H-PTS scheme of the CP-OFDM. For example, the BER value of H-PTS of the F-OFDM is 4.644×10^{-3} at SNR with 9 dB, while the H-PTS BER value of the CP-OFDM is 9.214×10^{-3} with SNR 9 dB. This is due to the transmitter filter in the F-OFDM system suppresses the sidelobes of the CP-OFDM signal which results in the interference reduction between the adjacent symbols.

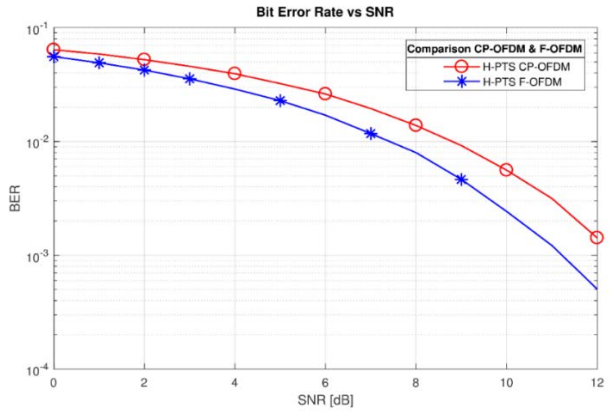

Fig. 14. BER of the OFDM and F-OFDM H-PTS, *N*=128, *M*=16.

7.2. The PSD evaluation of the H-PTS scheme

In this section, the performance of the power spectral density (PSD) of the CP-OFDM and F-OFDM transmitted signal has been examined. The number of subcarriers has been set as 128, while the baseband modulation is 16-QAM. Figure 15 shows that the OOBE of the original CP-OFDM signal starts at -31.47 dB, whereas the OOBE of the CP-OFDM signal using the H-PTS scheme starts at -35.72 dB, thereby the enhancement in the PSD performance for the H-PTS scheme is 4.25 dB compared with the original CP-OFDM signal. Likewise, Fig. 16 presents the PSD shape of the original signal of F-OFDM, and H-PTS based on F-OFDM, while the OOBE value of these signals start at -79.24 dB; thus, the PSD performance for both signals is almost alike. Furthermore, Fig. 17 indicates the PSD comparison of H-PTS with CP-OFDM and the same scheme with F-OFDM. It has been found that the PSD performance enhancement is 43.52 dB toward H-PTS with F-OFDM. This significant feature of the F-OFDM as a result of the suppression of the OOBE leakage of the CP-OFDM by the transmitter filter.

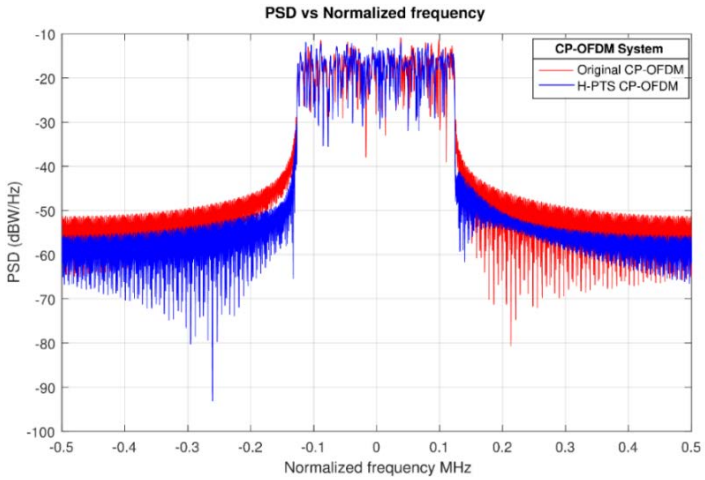

Fig. 15. PSD of the H-PTS scheme and the original signal in the CP-OFDM system, *N*=128, 16-QAM.

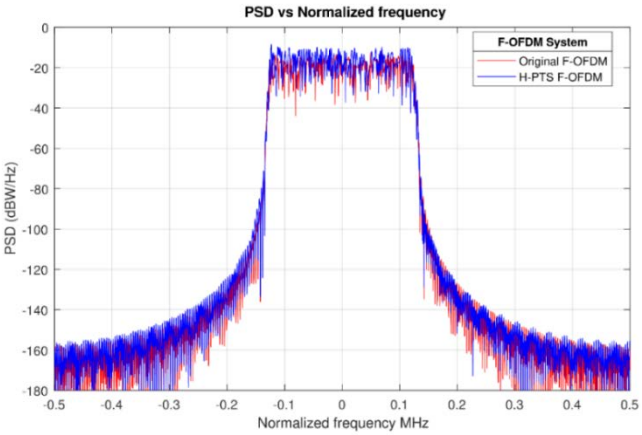

Fig. 16. PSD of the H-PTS scheme and the original signal in F-OFDM, *N*=128, 16-QAM.

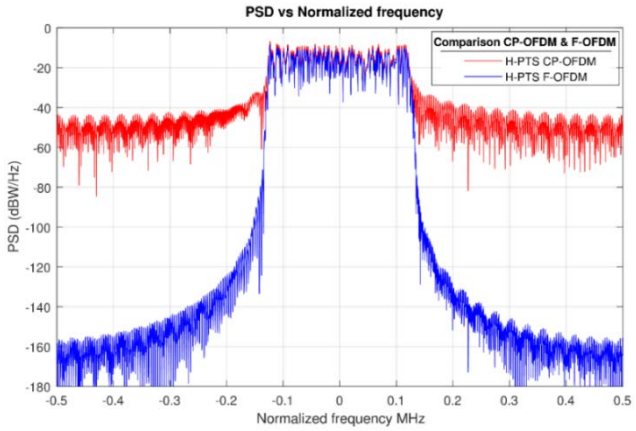

Fig. 17. The H-PTS performance comparison with CP-OFDM and F-OFDM systems, *N*=128, 16-QAM.

7.3. The H-PTS scheme computational complexity

In this subsection, the mathematical operations of H-PTS are calculated and compared with PR-PTS and some suggested techniques in the literature. As the *CC* level of the PR-PTS, H-PTS, and the proposed algorithms in the literature are the same value in the TD, the *CC* in the frequency domain (FD) will be adopted to evaluate the proposed algorithm and the other methods. Table 2 represents the FD complex addition and multiplication equations for PR-PTS, H-PTS, and the enhanced PTS methods in the literature. The related parameters to the *CC* calculations are: the subcarriers number N=[64, 128, 256, 512, 1024, 2048, 4096], the SBs number *V*=4, the concatenated factor *J*=2 that related to the Kang's et al. method [9], the conjugated SBs number *SS*=1 that correlated to Wang's et al. method [16], the length of the DFT block *E*=*N*/4 that related to Fulai's et al. method [13], and the difference between the IFFT stages and the intermediate data sequence stages (*n*-l)=5 that related to Lim's et al. method [15]. To avoid complexity, the oversampling dependent factor L, and the cyclic prefixes CP

number for all equations have been ignored because these values are the same in all calculations. In addition, it is essential to indicate the transmitter FD complexity equations with the PTS method.

Table 3 displays the number of operations of the complex multiplication and addition operations for various methods shown in Table 2. The results show that the *CC* of the H-PTS approach is the lowest among the techniques in Table 2, as shown in Figs. 18 and 19. For instance, when *N*=128 the number of the addition operations in H-PTS has been reduced by 52.06%, 17.64%, 30%, 57.57%, 62.67%, 48.14%, and 50% compared with PR-PTS or Chen and Chung [12], Kang et al. [9] or Wang et al. [10], Hong et al. [11], Fulai et al. [13], Jayashri et al. [14], Lim et al. [15], and Wang et al. [16], respectively. Besides, the number of the complex multiplications in the H-PTS algorithm has been reduced by 35.41%, 28%, 25%, 45.45%, 48.57, 33.33%, and 40% compared with the corresponding methods in Table 3. This improvement in *CC* is due to exploitation of the H-PTS algorithm the low complexity feature of the TE-PTS scheme and the structure of the H-PTS algorithm which combines TE-PTS and PR-PTS in parallel. Therefore, the H-PTS method is considered an effective algorithm to enhance the PAPR lessening performance with low *CC* level.

On the other hand, when *V*=4 and *W*=4, the side information bits of the H-PTS algorithm equal 12 bits per symbol, while the other methods in Table 3 have side information bits equal 6 bits per symbol. It is clear that the H-PTS algorithm has an excellent performance regarding of PAPR and *CC* performances, but this improvement at the expense of doubling the desired side bits for recovering the receiver original data.

Table 2. Frequency-domain complexities of H-PTS, PR-PTS, and the previous proposed approaches in the literature.

Method	C_{add}	C_{mult}
PR-PTS or Chen and Chung [12]	$V(N\log_2 N)$	$V\left(\frac{N}{2}log_2 N\right)$
H-PTS	$\frac{V}{2}\left[(N\log_2\frac{N}{2})+(\frac{N}{V}\log_2\frac{N}{2V})\right]$	$\frac{V}{2}\left[(\frac{N}{2}\log_2\frac{N}{2})+(\frac{N}{2V}\log_2\frac{N}{2V})+\frac{N}{2}\right]$
Kang et al. [9] or Wang et al. [10]	$V\left[\left(\frac{N}{V}log_2 J\right)+\left(N\log_2\frac{N}{VJ}\right)\right]$	$V\left[\left(\frac{N}{2V}log_2 J+N\right)+\left(\frac{N}{2}log_2\frac{N}{VJ}\right)\right]$
Hong et al. [11]	$\frac{V}{2}\left[\left(\frac{N}{V/2}log_2\frac{N}{V/2}\right)+(N\log_2 N)\right]$	$\frac{V}{2}\left[\left(\frac{N}{V}log_2\frac{N}{V/2}+N\right)+\left(\frac{N}{2}log_2 N\right)\right]$
Fulai et al. [13]	$V[(E\log_2 E)+(N\log_2 N)]$	$V\left[\left(\frac{E}{2}log_2 E\right)+\left(\frac{N}{2}log_2 N\right)\right]$
Jayashri et al. [14]	$\left[\frac{3N}{2}log_2 N-N+1\right]+V(N\log_2 N)$	$(V+1)\left[\frac{N}{2}log_2 N\right]$
Lim et al. [15]	$(2^n\times n)+[2^n\times V(n-l)]$	$(2^{n-1}\times n)+[2^{n-1}\times V(n-l)]$
Wang and Cao [16]	$V(N\log_2 N)$	$V\left[\frac{N}{2}log_2 N\right]+(SS\times N)$

Table 3. The frequency-domain computational complexity of H-PTS and the other PTS methods in the literature, V = 4.

N	PR-PTS [12]		H-PTS		[9] or [10]		[11]	
	C_{add}	C_{mult}	C_{add}	C_{mult}	C_{add}	C_{mult}	C_{add}	C_{mult}
64	1536	768	736	496	832	672	1088	672
128	3584	1792	1792	1152	2176	1600	2560	1536
256	8192	4096	4224	2624	5376	3712	5888	3456
512	18432	9216	9728	5888	12800	8448	13312	7680
1024	40960	20480	22016	13056	29696	18944	29696	16896
2048	90112	45056	49152	28672	67584	41984	65536	36864
4096	196608	98304	108544	62464	151552	92160	143360	79872

N	Fulai et al. [13]		Jayashri et al. [14]		Lim et al. [15]		Wang and Cao [16]	
	C_{add}	C_{mult}	C_{add}	C_{mult}	C_{add}	C_{mult}	C_{add}	C_{mult}
64	1792	896	2049	960	1664	832	1536	832
128	4224	2112	4801	2240	3456	1728	3584	1920
256	9728	4864	11009	5120	7168	3584	8192	4352
512	22016	11008	24833	11520	14848	7424	18432	9728
1024	49152	24576	55297	25600	30720	15360	40690	21504
2048	108544	54272	121857	56320	63488	31744	90112	47104
4096	237568	118784	266241	122880	131072	65536	196608	102400

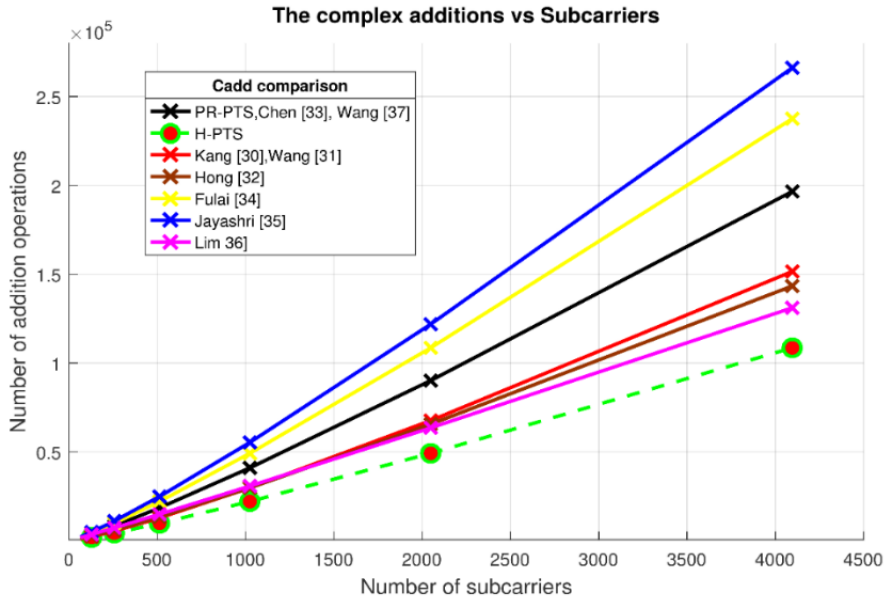

Fig. 18. The Comparison of various methods in Table 3 for various number of complex additions.

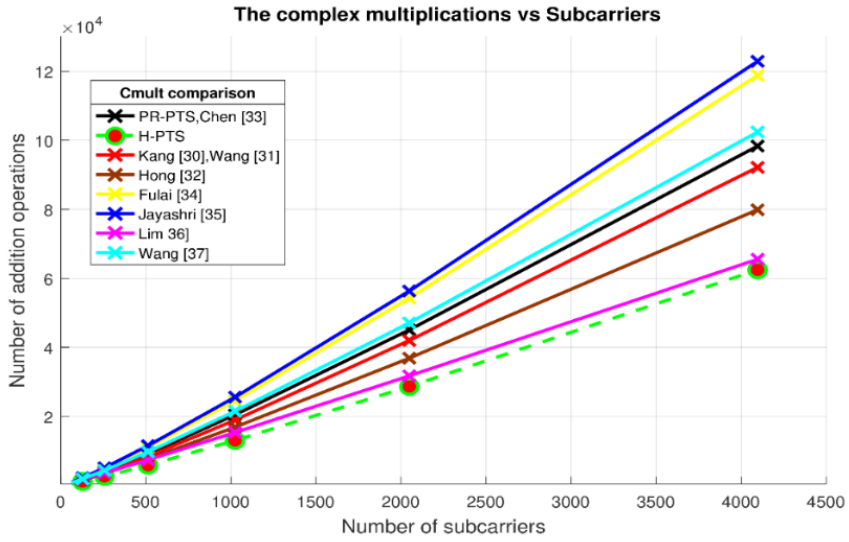

Fig. 19. The Comparison of various methods in Table 3 for various number of complex multiplications.

8. Conclusions

In conclusion, a new hybrid algorithm named H-PTS has been adopted to the CP-OFDM and F-OFDM systems for enhancing the *CC* level and the PAPR reduction capacity. The new algorithm depended on the combination of two types of the SBs segmentation schemes PR-PTS and TE-PTS in parallel. The new algorithm has been evaluated based on the CP-OFDM and F-OFDM systems. The simulated results demonstrate that the PAPR reduction performance of the proposed algorithm outperforms that of the PR-PTS method by 0.43 dB, while the *CC* has been reduced by 52% at the number of subcarriers of 128. Moreover. The BER performance of the H-PTS algorithm and the original signal is identical. Therefore, the H-PTS algorithm can be considered the best algorithm in the PTS method for improving the PAPR reduction capacity with low *CC* level.

Nomenclatures

B	Number of phase factors
CC	Computational complexity
FL	Filter length
L	Oversampling number
N	Subcarrier number
V	Number of subblock
W	Number of permissible phase rotation factors
$x(n)$	Discrete baseband OFDM signal

Greek Symbols

α	Roll-off factor

Abbreviations

BER	Bit Error Rate
FBMC	Filter Bank Multicarrier
IFFT	Inverse Fast Fourier Transform
OOBE	Out-of-Band Emission
PAPR	Peak-to-Average-Power Ratio
UFMC	Universal Filtered Multicarrier

References

1. Ahmed, S.; and Li, Z. (2013). Complexity reduced detection for MIMO–OFDMA uplink with distinct frequency offsets from each user. *Physical Communication*, 9, 125-134.
2. Taspinar, N.; and Tokur, Y. (2016). PAPR reduction using genetic algorithm in lifting-based wavelet packet modulation systems. *Turkish Journal of Electrical Engineering and Computer Sciences*, 24(1), 184-195.
3. Jawhar, Y.; Abdulhasan, R.; and Ramli, K. (2016). Influencing parameters in peak to average power ratio performance on orthogonal frequency-division multiplexing system. *ARPN Journal of Engineering and Applied Sciences*, 11, 4322-4332.
4. Anoh, K.; Adebisi, B.; Rabie, M.; and Tanriover, C. (2018). Root-based nonlinear companding technique for reducing PAPR of precoded OFDM signals. *IEEE Access*, 6, 4618-4629.
5. Yi, W.; and Leib, H. (2017). OFDM symbol detection integrated with channel multipath gains estimation for doubly selective fading channels. *Physical communication*, 22, 19-31.
6. Singh, A.; and Singh, H. (2016). Peak to average power ratio reduction in OFDM system using hybrid technique. *Optik-International Journal for Light and Electron Optics*, 127(6), 3368-3371.
7. Fakhraie, M.; and Nader-Esfahani, S. (2009). Performance evaluation of IEEE 802.20 PHY layer. *Proceedings of the IEEE International Conference on Computer Engineering and Technology (ICCET'09)*. Singapore, 161-169.
8. Joo, S.; Kim, H.; No, S.; and Shin, J. (2017). New PTS schemes for PAPR reduction of OFDM signals without side information. *IEEE Transactions on Broadcasting*, 63(3), 562-570.
9. Kang, G.; Kim, G.; and Joo, K. (1999). A novel subblock partition scheme for partial transmits sequence OFDM. *IEEE Transactions on Broadcasting*, 45(3), 333-338.
10. Wang, M.; Xiao, J.; Yuan, C.; Tian, Y.; and Zhang, L. (2017). A new low-complexity subblock segmentation method for PTS OFDM. *Proceedings of the 2nd IEEE International Conference on Advanced Information Technology, Electronic and Automation Control (IAEAC)*. Chongqing, China, 2408-2411.
11. Hong, C.; Qin, Q.; and Chao, T. (2013). An PTS optimization algorithm for PAPR reduction of OFDM system. *Proceedings of the IEEE International Conference on Mechatronic Sciences, Electric Engineering and Computer (MEC).* Shenyang, China, 3775-3778.

12. Chen, H.; and Chung, C. (2018). A PTS technique with non-disjoint sub-block partitions in M-QAM OFDM systems. *IEEE Transactions on Broadcasting*, 64(1), 146-152.
13. Fulai, Z.; Luokun, L.; and Jinjin, Y. (2014). DFT-spread combined with PTS method to reduce the PAPR in VLC-OFDM system. *Proceedings of the 5th IEEE International Conference on Software Engineering and Service Science*. Beijing, China, 629-632.
14. Jayashri, R.; Sujatha, S.; and Dananjayan, P. (2016). DCT based partial transmit sequence technique for PAPR reduction in OFDM Transmission. *ARPN Journal of Engineering and Applied Sciences*, 10(5), 2182-2186.
15. Lim, W.; Heo, J.; No, S.; and Chung, H. (2006). A new PTS OFDM scheme with low complexity for PAPR reduction. *IEEE Transactions on Broadcasting*, 52, 77-82.
16. Wang, L.; and Cao, Y. (2008). Sub-optimum PTS for PAPR reduction of OFDM signals. *IEEE Electronics Letters*, 44(15), 921-922.
17. Jawhar, Y.; Ramli, K.; Taher, M.; Shah, N.; Audah, L.; Ahmed, M.; and Abbas, T. (2018). New low complexity segmentation scheme of partial transmit sequence technique to reduce the high PAPR value in OFDM systems. *ETRI Journal*, 40(6), 1-15.
18. Jawhar, Y.; Ramli, K.; Taher, M.; Audah, L.; Shah, N.; Ahmed, M.; and Hammoodi, A. (2018). An enhanced partial transmit sequence based on combining hadamard matrix and partitioning schemes in OFDM systems. *International Journal of Integrated Engineering*, 10(3), 1-7.
19. Jawhar, Y.; Shah, N.; Taher, M.; Ahmed, M.; Ramli, K.; and Abdulhasan, R. (2017). A low PAPR performance with new segmentation schemes of partial transmit sequence for OFDM systems. *IJAAS International Journal of Advanced and Applied Sciences*, 4(4), 14-21.
20. Jawhar, Y.; Ramli, K.; Ahmed, M.; Abdulhasan, R.; Farhood, H.; and Alwan, M. (2018). A new partitioning scheme for PTS technique to improve the PAPR performance in OFDM systems. *International Journal of Engineering and Technology Innovation*, 8(3), 217-227.
21. Elshirkasi, A. M.; Siddiqi, M. U.; and Habaebi, M. H. (2015). Generalized discrete Fourier transform based improvement of partial transmit sequence scheme to reduce PAPR in OFDM systems. *Journal of Theoretical and Applied Information Technology*, 76(1), 76-81.
22. Bodinier, Q.; Bader, F.; and Palicot, J. (2016). Coexistence of filter banks and CP-OFDM: What are the real gains? *Proceedings of the 13th IEEE International Symposium on Wireless Communication Systems (ISWCS)*. Poznan, Poland, 628-632.
23. Ochiai, H.; and Imai, H. (2001). On the distribution of the peak-to-average power ratio in OFDM signals. *IEEE Transactions on Communications*, 49(2), 282-289.
24. Jawhar, Y.; Shah, N.; Taher, M.; Ahmed, M.; and Ramli, K. (2017). An enhanced partial transmits sequence segmentation schemes to reduce the PAPR in OFDM systems. *International Journal of Advanced Computer Science and Applications (IJACSA)*, 7(12), 66-75.
25. Liu, Y.; Chen, X.; Zhong, Z.; Ai, B.; Miao, D.; and Zhao, Z. (2017). Waveform design for 5G networks: Analysis and comparison. *IEEE Access*, 5, 19282-19292.

26. Weitkemper, P.; Bazzi, J.; Kusume, K.; Benjebbour, A.; and Kishiyama, Y. (2016). Adaptive filtered OFDM with regular resource grid. *Proceedings of the IEEE International Conference on Communications Workshops (ICC)*. Kuala Lumpur, Malaysia, 462-467.
27. Gerzaguet, R.; Bartzoudis, N.; Baltar, G.; Berg, V.; Doré, B.; and Kténas, D. (2017). The 5G candidate waveform race: a comparison of complexity and performance. *EURASIP Journal on Wireless Communications and Networking*, 13, 1-14.
28. Wang, J.; Jin, A.; Shi, D.; Wang, L.; Shen, L.; and Wu, D. (2017). Spectral efficiency improvement with 5G Technologies: Results from field tests. *IEEE Journal on Selected Areas in Communications*, 35, 1867-1875.
29. Wu, D.; Zhang, X.; Qi, J.; Gu, L.; Saito, Y.; and Benjebbour, A. (2016). A field trial of f-OFDM toward 5G. *IEEE in Globecom Workshops (GC Workshops)*. Washington, DC, USA, 1-6.
30. Guan, P.; Wu, D.; Tian, T.; Zho, J.; Zhang, X.; and Gu, L. (2017). 5G field trials: OFDM-based waveforms and mixed numerologies. *IEEE Journal on Selected Areas in Communications*, 35, 1234-1243.
31. Schaich, F.; and Wild, T. (2014). Waveform contenders for 5G-OFDM vs. FBMC vs. UFMC. Proceedings *of the 8th IEEE International Conference on Communications, Control and Signal Processing (ISCCSP)*. Athens, Greece, 457-460.
32. Lee, S.; Cho, J.; Woo, Y.; No, S.; and Shin, J. (2016). Low-complexity PTS schemes using OFDM signal rotation and pre-exclusion of phase rotating vectors. *IET Communications*, 10(5), 540-547.
33. Xia, L.; Yue, X.; Youxi, T.; and Shaoqian, L. (2007). A novel method to design phase factor for PTS based on pseudo-random sub-block partition in OFDM system. *Proceedings of the 66th IEEE International Conference on Vehicular Technology*. Baltimore, USA, 1269-1273.
34. Sandoval, F.; Poitau, G.; and Gagnon, F. (2017). Hybrid peak-to-average power ratio reduction techniques: Review and performance comparison. *IEEE Access*, 5, 27145-27161.
35. Tani, K.; Medjahdi, Y.; Shaiek, H.; Zayani, R.; and Roviras, D. (2018). PAPR reduction of post-OFDM waveforms contenders for 5G and beyond using SLM and TR algorithms. *Proceedings of the 25th IEEE International Conference on Telecommunications (ICT)*. St. Malo, France, 104-109.
36. Jawhar, Y.; Ramli, K.; Mustapha, A.; Mostafa, S.; Shah, N.; and Taher, M. (2019). Reducing PAPR with low complexity for 4G and 5G waveform designs. *IEEE Access*, 7, 97673-97688.